The catalytic mechanism of fungal lytic polysaccharide monooxygenases investigated by first principles calculations

Luca Bertini,[1] Raffaella Breglia,[2] Matteo Lambrughi,[3] Piercarlo Fantucci,[1] Luca De Gioia,[1] Marco Borsari,[4] Marco Sola,[3] Carlo Augusto Bortolotti,[3]* Maurizio Bruschi[2]*

[1] Department of Biotechnology and Biosciences, University of Milan-Bicocca, Piazza della Scienza 2, 20126 Milan, Italy

[2] Department of Earth and Environmental Sciences, University of Milan-Bicocca, Piazza della Scienza 1, 20126 Milan, Italy

[3] Department of Life Sciences, University of Modena and Reggio Emilia, Via Campi 103, 41125, Modena, Italy

[4] Department of Chemical and Geological Sciences, University of Modena and Reggio Emilia, Via Campi 103, 41125, Modena, Italy

* E-mail: carloaugusto.bortolotti@unimore.it; maurizio.bruschi@unimib.it

ABSTRACT

Lytic polysaccharide monooxygenases (LPMOs) are copper-containing enzymes that facilitate the degradation of recalcitrant polysaccharides by oxidative cleavage of glycosidic bonds. They are gaining a rapidly increasing attention as key players in biomass conversion, especially for the production of second generation biofuels. The elucidation of the detailed mechanism of the LPMO reaction is a major step towards the assessment and optimization of LPMO efficacy in industrial biotechnology, paving the way to the utilization of sustainable fuel sources. Here, we used Density Functional Theory (DFT) calculations to study the reaction pathways suggested to date, exploiting a very large active site model for a fungal AA9 LPMO and using a celloheptaose unit as a substrate mimic. We identify a copper oxyl intermediate as responsible for hydrogen abstraction from the substrate, followed by a rapid, water assisted hydroxyl rebound leading to substrate hydroxylation.

INTRODUCTION

The recently discovered lytic polysaccharide monooxygenases (LPMOs, also known as PMOs) are metalloenzymes, featuring a single copper centre, which boost biomass degradation by oxidative polysaccharide chain breakage via oxidation at C1 and/or C4.[1–6] They have been gaining rapidly increasing attention in the last few years. [4,7–11] Focus has been mainly put on the use of LPMOs in enzymatic cocktails for the production of second generation biofuels, made from non-edible biomass such as agricultural and forest residues, crops not used for food purposes, as well as industrial and urban wastes.[12,13] Besides their potentially crucial role in the long overdue issue of reduction of greenhouse emissions by utilization of low-carbon sources,[14] these enzymes also pose challenging fundamental questions, related to their unusual catalytic and structural properties that make them peculiar within the framework of Cu active sites in biological systems.

The LPMO active site is composed by a copper atom coordinated equatorially by the imidazole nitrogen atoms of two histidines, one of these being the N-terminal residue, and the nitrogen atom of the terminal amine, in a so-called histidine brace motif.[4] When copper is in the oxidized Cu(II) state, the coordination is completed by the oxygen atoms of a conserved Tyr residue and a water molecule.

Based on their substrate specificity and on the host organism, LPMOs are currently classified into four Auxiliary Activity (AA) families in the Carbohydrate-Active enZyme (CAZy) database:[15] cellulose- and hemi-cellulose active fungal LPMOs (forming the AA9 family); chitin- and cellulose-active bacterial LPMOs (AA10); chitin-active fungal LPMOs (AA11) and fungal starch-degrading LPMOs (AA13).

Although the structural features that underlie substrate binding and specificity by LPMOs are yet to be fully elucidated, a deeper level of understanding is being achieved thanks to the increasing number of LPMOs structures deposited in the PDB database: this allows for a structural comparison of the LPMOs family members, and for the identification of conserved/varying regions that are involved in substrate binding and (regio)selectivity. In AA9 LPMO (hereafter LPMO9s), the substrate-binding surface is mostly constituted by highly variable Loop 2 (L2) and loops LS and LC. These regions feature aromatic residues,[9,16–19] and the spacing between them typically matches the distance between polysaccharide units,[16,19] so that they are indicated as directly involved in the ligand binding. Major insights were gained thanks to the crystal structure of an LPMO9 with bound oligosaccharide,[20] revealing that hydrogen bonds between surface exposed Asn and His residues also play a crucial role in the interaction with the substrate, together with an electrostatic interaction between the N-terminal His1 imidazole and the ring oxygen of the sugar occupying the +1 site.

NMR investigations followed by docking studies on a closely related LPMO member also indicated His155, Ala80, His83 and Tyr204 residues as involved in the ligand binding.[21]

The LPMO reaction results in the breakage of the glycosidic bond and, depending on whether oxidation takes place at C1 or C4, yields sugar lactones or ketoaldoses, respectively. In both cases, the reaction proceeds via oxidative cleavage of a C-H bond by atmospheric O_2[22] or, as very recently proposed, by H_2O_2,[23] requiring the H abstraction from the carbon atom and subsequent hydroxylation to give a C-OH species. Assuming the enzyme in the Cu(I) reduced state and O_2 as oxidant, the substrate hydroxylation catalysed by LPMOs further requires two protons and two electrons, whereas H_2O_2 can react without additional protons and electrons. In both cases substrate hydroxylation is accompanied by elimination of a water molecule. At present, there is no consensus on what is the exact mechanism underlying the LPMO catalytic activity. Preliminary, and somehow contrasting, hypotheses on the possible reaction path came from spectroscopic,[24] crystallographic[25] and computational[24,26] insights. In particular, two studies describing DFT-based investigations[24,26] contributed to the modelling of some of the intermediate species possibly involved in the LPMO catalytic cycle with O_2 as oxidant. Kjaergaard et al.[24] reported calculated structures for both Cu(II) and Cu(I) states of an LPMO9 enzyme: calibrating their calculations based on spectroscopic (X-ray absorption near edge structure and extended X-ray absorption fine structure) measurements, they describe a significant rearrangement in the copper coordination upon reduction, with Cu(I) becoming three-coordinated by the histidine-brace nitrogens. Moreover, the authors investigated the first step in the LPMO reaction, i.e. the binding of dioxygen to Cu(I), leading to the formation of a Cu(II)-superoxide species by inner-sphere reduction. The most stable structure obtained by their calculations displays the superoxide ion bound end-on to Cu(II). Kim et al.[26] used DFT to explore the whole LPMO reaction mechanism, investigating two hypothesized reaction pathways differing for the intermediate species that abstracts a hydrogen atom from the substrate: their calculations

4

indicate that the substrate hydroxylation proceeds via an oxygen-rebound mechanism where a copper-oxyl intermediate is responsible for breaking the C1-H (or C4-H) bond in the substrate.

Despite the insights gained so far, the open questions are still largely outnumbering the undisputed evidences concerning the LPMO catalytic mechanism. In particular, the main unsolved issues concern i) to what extent the presence of the sugar might promote oxidative addition of the oxidant (O_2 or H_2O_2) to Cu(I); ii) the identity of the intermediate that performs the hydrogen atom abstraction (HAA hereafter) step and iii) whether the necessary electrons and protons are transferred separately or in combined steps.

In this paper, we investigate the main LPMO reaction pathways hypothesized so far using DFT calculations. As a prototype system, we built a large active site model of an AA9-LPMO from *Neurospora crassa* (*Nc*LPMO9M), calculating and comparing the potential energy surfaces of the different proposed reaction schemes. We aimed at providing new insights into the monooxygenase activity of fungal LPMOs, underlying the role played by second sphere residues in assisting the catalytic mechanism.

METHODS

The active site model

The starting structure for the QM calculations was based on the X-ray geometry of the AA9-LPMO solved by Li *et al.* (PDBcode: 4EIS, chain B).[25] In this structure, the Cu(II) ion is five-coordinated in a roughly square-pyramidal geometry by the two Nε of the imidazole rings of His1 and His82 residues, the N amine atom of the His1 N-terminal, the hydroxyl moiety of Tyr171 and a water molecule.

5

In our investigation, we considered a very large model of about 420 atoms (see Fig. 1 and Supplementary Fig. 1 and 2). The model is composed by the active site of the protein with first and second coordination sphere residues and by the substrate modelled by a cellulose oligomer of seven monomeric units (celloheptaose). The model also includes the side chain of two Tyr residues (Tyr20 and Tyr210) lying on the flat cellulose binding surface of the protein, that are located more than 14 Å far from the copper ion. The inclusion of these two residues in the model was inspired by the fact that conserved aromatic amino acids on the flat LPMO face were suggested to be responsible *in vivo* for the weak interactions that yield substrate binding.[16,25,27] Indeed, the aromatic ring of these two residues interacts with the peripheral units of the celloheptaose allowing the substrate to be close enough to enter into the reaction without imposing any constraints to the polysaccharide atoms. It is important to note that, in our model, the role of these two residues is not to accurately model the binding of the substrate to the surface of the enzyme, but to assist the anchoring the substrate in proximity of the active site.
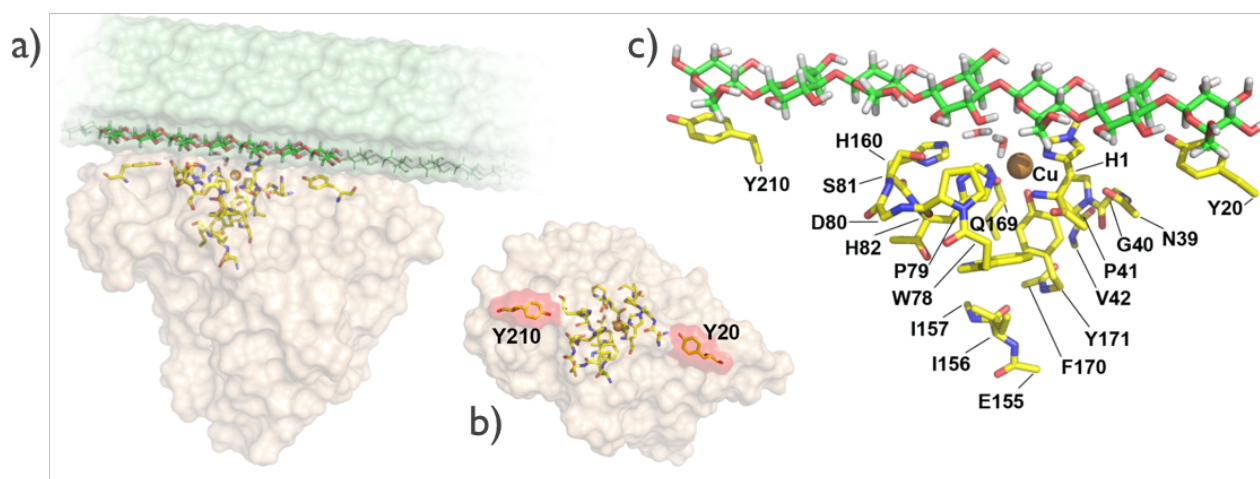

Figure 1: a) Cartoon representation of the *N. crassa* LPMO (light yellow) docked to a cellulose (light green) surface. The seven D-glucose units of the celloheptaose, used to model the substrate in our calculations, are displayed as sticks, while the other sugar monomers completing the cellulose chain are shown as thin green lines. The copper atom is represented by a brown sphere; all the other

atoms are shown as sticks, with the usual colour coding (white for H, blue for N, red for O), except for C atoms, which are green for the substrate and yellow for the protein. The H atoms of the protein active site are omitted for the sake of clarity. b) Semi-transparent, bottom view of the flat putative substrate binding surface of LPMO. The solvent accessible surface (SAS) of two conserved Tyr residues Y20 and Y210 is coloured in pink. c) Detailed representation of the active site model used.

The approach adopted in building the copper active site model is that of including a large enough number of atoms to allow coordination rearrangements during the reaction with the substrates (O_2 and celloheptaose). The importance to consider such second coordination sphere residues in the cluster model to properly describe the catalytic mechanism has been discussed in several recent studies.[28–31] We included in the model residues reaching deep within the antiparallel beta sheet region of the LPMO core to minimize the number of constraints at the protein active site. This implies that the copper first shell residues (His1, His82, Tyr171, apical H_2O) are allowed to freely relax during geometry optimizations, in particular Tyr171, that is believed to detach from the metal upon Cu(I) formation. To this end, the N_3O Cu coordination was embedded in a 14-residue "second shell" (encompassing Asn39, Gly40, Pro41, Val42, Trp78, Pro79, Asp80, Ser81, Glu155, Ile156, Ile157, His160, Gln169, Phe170), which avoids unrealistic conformational rigidity imposed by the constraints to the first shell residues. When possible, the side chains were simplified in order to save CPU time. Finally, the outermost carbon atoms of the second shell residues were kept fixed at their 4EIS-B.pdb structure during geometry optimizations. Details of the residues included in the model and of the constrained atoms are reported in Supplementary Fig. 1 and 2.

Geometry optimizations to transition states have been first carried out on a smaller model in order to perform eigenvector following technique with only a very limited number of atom constraints. The model includes the first shell residues (His1, His82 and Tyr171) and the substrate is mimicked by a cellobiose unit. The TS structures have then been inserted into the large model and geometry

optimizations of such model have been carried out by constraining the few atoms that move along the reaction coordinate to the positions calculated in the small model (see Supplementary Fig. 3 for the atoms constrained in each TS). Finally, several structures connecting the reactant, the TS and the product have been generated assuming a linear reaction coordinate in order to obtain the entire reaction profile.

Computational Details

Computations were performed in the framework of the Density Functional Theory (DFT) using the pure Gradient Generalized Approximation BP86 functional.[32,33] The def-SVP basis set was adopted for the second shell residues and for the peripheral units of celloheptaose, while higher quality def-TZVP[34] basis set was adopted for Cu, first shell residues, dioxygen, and the two units of the celloheptaose directly involved in the catalytic mechanism. Resolution-of-Identity (RI) technique was adopted for pure functionals in order to save CPU time.[35] All calculations were carried out using the TURBOMOLE suite of programs.[36] Such computational approach has already been found to be appropriate for the correct representation of the electronic properties of Cu-peptide interactions.[37,38] In the framework of the unrestricted formalism, the unpaired spin electronic structures were modelled with the broken symmetry (BS) approach introduced by Noodleman *et al*.[39,40] that consists in the localization of opposite spins of the mono-determinant wave function in different parts of the molecule. In this work, the BS singlet species within this formalism have been considered and the resulting electronic structures have been checked by computing spin and charge populations using the Mulliken and the NBO schemes, respectively.[41–43]

To check the effects of spin contamination in the BS solutions, we project out the higher spin state from the singlet BS solution obtaining a pure-spin state energy. This latter has been computed by applying the Yamaguchi equation:[44]

$$^{LS}E = \frac{^{BS}E\left(^{HS}\langle S^2\rangle - {}^{LS}\langle S^2\rangle\right) - {}^{HS}E\left(^{BS}\langle S^2\rangle - {}^{LS}\langle S^2\rangle\right)}{^{HS}\langle S^2\rangle - {}^{LS}\langle S^2\rangle}$$

where $^{HS}\!<\!S^2\!>$ and $^{BS}\!<\!S^2\!>$ are the total spin operator of the high-spin (triplet) and the broken-spin (open shell singlet) states, respectively. $^{LS}\!<\!S^2\!>$ is the total spin operator of closed shell singlet state, which is equal to 0.

The species, in which the hydrogen atom of the substrate has been transferred to the active site reproducing the HAA mechanism, has been calculated as singlet BS solutions, in which two electrons with opposite spin were localized on the substrate and active site, respectively. In the rebound mechanism (see the Results section), in which the OH group spontaneously moved to the substrate, the BS solution converged to the pure singlet one after several geometry optimization steps.

Transition states search has been performed on the small model according to a pseudo Newton-Raphson procedure, and the TSs have been characterized by a full vibrational analysis. The presence of constrained atoms resulted in the occurrence of several imaginary frequencies. However, the eigenvector corresponding to the reaction coordinate was easily identified as the one with an eigenvalue much lower than the other negative eigenvalues.

In order to verify the consistency of the results, we have also carried out geometry optimizations of the LPMO-Cu(II), LPMO-Cu(I) and LPMO-Cu(II)-O-O•$^{-}$ using the B3LYP[33,45] hybrid exchange-correlation functional with the same TZVP-SVP basis set. The results obtained using the B3LYP functional are consistent with those obtained by using the BP86 scheme, and, for the sake of clarity, will be not further commented in the text (see Supplementary Tables 1 and 2 for the comparison of the geometries calculated using the different schemes).

Nomenclature

In the following, LPMO-Cu(II) and LPMO-Cu(I) protein structures are indicated by $\mathbf{P_{OX}}$ and $\mathbf{P_{RED}}$ labels, respectively. These labels were substituted by $\mathbf{P_{O2}}$ when O_2 binds the Cu atom, while the tag **RH** is added when the celloheptaose is included in the model. The investigated intermediates following O_2 and celloheptaose binding to the LPMO enzyme, are labelled according the general scheme $\mathbf{K_x\text{-}J\text{-}RH}$, where K is a generic number referring to the path along which this intermediate is formed, x indicates the chemical nature of the species coordinated to the Cu atom and J the nature of the species that dissociates from the active site. The RH tag is substituted by $\mathbf{R\bullet}$ when a hydrogen atom is abstracted from the C4 atom of the celloheptaose and by $\mathbf{RO^-}$, **ROH** and **ROOH** when this atom is replaced by oxyl, hydroxyl and peroxyl species, respectively. Isomers of the investigated computational models are pointed out by adding the tag **iso**.

RESULTS

Validation of the model

In the present work, the active site model includes a greater number of atoms, compared to those used for previously reported computational investigations of the LPMO mechanism. We decided to build such a large model, despite its computational cost, to take into account second coordination sphere effects and to avoid introducing any constraint on the first coordination sphere residues. Despite being clearly less relevant than that deriving from the first coordination sphere, the importance of secondary sphere residues in determining properties and function of metalloproteins has been demonstrated for several systems,[46] including those that activate dioxygen.[47] In the case of LPMOs, a very recent work from Span *et al.* revealed the crucial role played by secondary coordination sphere in a fungal LPMO: in particular, they identified His and Gln amino acids,

belonging to a H-bond network conserved in all fungal LPMO families, as important residues for oxygen activation.[48]

Our model was validated by comparing the optimized Cu(II) and Cu(I) geometries with experimental data. The optimized active site structure for the oxidized, LPMO-Cu(II) form (P_{OX}), preserves the square pyramidal coordination mode of the experimental X-ray structure. In particular, N(-NH$_2$), Nδ(His1), Nϵ(His82) and O(H$_2$O) form the four corners of the equatorial plane and O(Tyr171) serves as apical ligand (see Fig. 2 and Supplementary Fig. 4). All the bond distances with the Cu atom are within 0.15 Å with respect to the X-ray values, with the only exception of the Cu-O(Tyr171) distance, which is about 0.25 Å longer in the calculated structure. Slight distortions are observed, as witnessed by the 29° dihedral angle between the two planes (O-N-N and N-N-N) formed by the equatorial ligands. The reliability of our model is further supported by the calculated root mean square deviation (RMSD) of the model structure (including all atoms) with the crystallographic structure, that is as low as 0.732 Å. (see Supplementary Fig. 5 for the overlay of calculated and experimental structures).
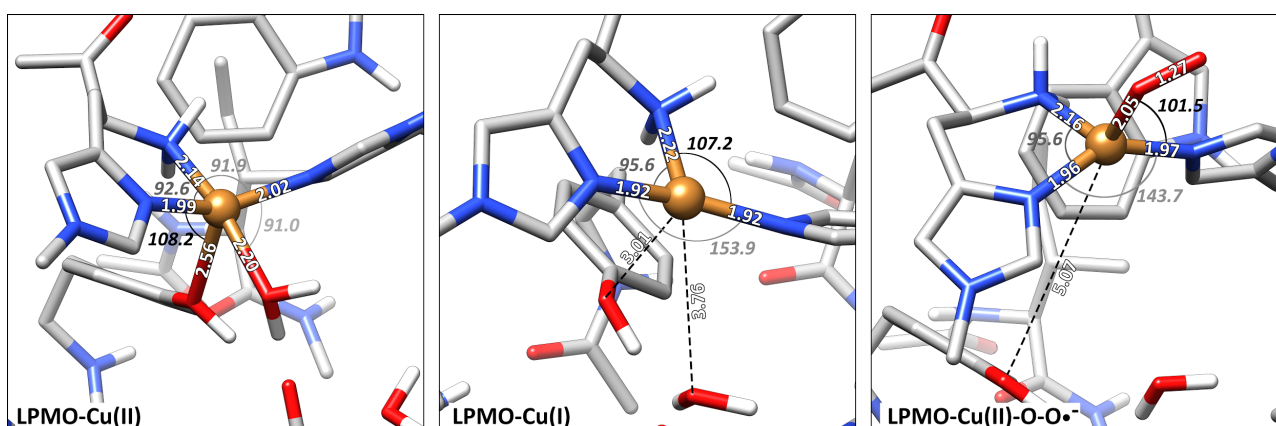

Figure 2: Coordination geometry of the copper ion in the LPMO-Cu(II) (P_{OX}), LPMO-Cu(I) (P_{RED}) and LPMO-Cu(II)-O-O•$^-$ (P_{O2}) species with selected interatomic distances (in angstroms) and angles (in degrees). For the sake of clarity, aliphatic hydrogen atoms are not shown.

11

The crystallographic structure of the reduced Cu(I) form (**P$_{RED}$**), obtained by X-ray photoreduction on an AA10 LPMO from *Enterococcus faecalis*,[49] shows a significant rearrangement of copper coordination. The Cu(I) site is three-coordinate, with the copper ion bound by the same three N atoms as in the oxidized form, in a T-shaped geometry (N-Cu-N angle with the two histidines of 154°). Such a coordination for Cu(I)-LPMO was further confirmed by an Extended X-ray Absorption Fine Structure (EXAFS) investigation performed on a AA9 LPMO from *Thermoascus aurantiacus*.[24] Notably, our optimized geometry of LPMO-Cu(I) closely reproduces the crystallographic structure, as both O ligands in LPMO-Cu(II) move away from the copper ion upon reduction: the Cu-O(Tyr171) distance increases up to 3.01 Å, and the water molecule providing the equatorial O ligand in LPMO-Cu(II) also leaves the first coordination sphere (see Fig. 2). In the optimized structure, the side chain carbonyl oxygen of Gln169 forms a H-bond with the hydroxyl group of Tyr171. Notably, such interaction has been also inferred by X-band EPR measurements on a mixed C1-C4 oxidizer LPMO from *Myceliophthora thermophila*.[48]

The dissociated water molecule is held close to the active site by the formation of H-bonds with the side chain amidic nitrogen of Gln169 and the Nδ atom of His160. In addition, the change to a T-shaped geometry upon reduction and the calculated N-Cu distances for Cu(I)-LPMO (1.92 Å for both Nδ(His1)-Cu and Nε(His82)-Cu and 2.22 Å for Cu-N(-NH$_2$)) are in excellent agreement with spectroscopic[24] results and crystallographic measurements.[25] It should be noted that these results are similar to those obtained by Kjaergaard *et al.*[24] in a previous DFT investigation, but at variance with the four-coordinate Cu(I)-LPMO structure proposed by Kim *et al.*[26], the latter being in contrast with experimental findings concerning reduced LPMOs. This discrepancy might be due to the small size and the large number of constraints of the model adopted by these authors, as well as to the different level of theory adopted in their calculations. A decrease of 0.33e of the total charge on copper was observed between the optimized Cu(II) and Cu(I) structures. This value is in line with

those recently obtained for reduction of Cu amyloid peptide systems,[37] and indicates a reduction process in which the extra electron occupies molecular orbitals mainly localized on the metal centre. The good agreement between calculated and experimental structural data for the copper site of LPMO in both oxidation states is an essential requisite to ascertain the reliability of the present model in predicting structural changes along the putative steps of the catalytic mechanism.

The binding of celloheptaose to the LPMO-Cu(II) enzyme (**P_{OX}-RH**; see Supplementary Fig. 6) in our larger model occurs through the interaction of two glucosyl units with the two lateral Tyr residues and a H-bond between the oxygen atom of one of the CH_2OH groups of the celloheptaose and the hydrogen atom of the Ser81 hydroxyl group. The Ser81 side chain also forms a second H-bond interaction with the -NH of the His82 imidazole ring. This H-bond network contributes to anchor the substrate to the enzyme. The orientation of the substrate and its distances from the anchoring amino-acids are also in reasonable agreement with the recent crystallographic structure obtained for an AA9 LPMO from *Lentinus similis* in the presence of polysaccharide substrate.[20] In particular, the H-bond interaction of the Ser81 hydroxyl group with the substrate is well reproduced by the X-ray structure, with the $O_{Ser81}(H)-O_{Subst}$ distance in the model (2.67 Å) perfectly matching the experimental value (2.7 Å). In addition, the average C-C distances between the Tyr aromatic ring and the interacting glucosyl unit are 4.17 and 4.54 Å (see Supplementary Fig. 2), and both values are comparable with the crystallographic value (3.7 Å for the C-C distance between Tyr203 and anchored glucosyl unit of cellohexaose).[20]

The O_2 binding to the Cu ion is facilitated by the concomitant binding of the substrate

Following Cu(II) reduction and consequent transition to a three-coordinate geometry, the LPMO catalytic mechanism is believed to proceed via binding of O_2 to form a LPMO-Cu(II)-O-O•⁻ superoxo intermediate (**P_{O2}**). We have therefore investigated the binding of O_2 at the LPMO-Cu(I)

active site. At this stage of the pathway, it is also relevant to evaluate the effect of substrate binding on the coordination of O_2.

The two possible S=1 and S=0 spin states (open shell singlet, broken symmetry (BS) corrected) of the O_2-adducts LPMO-Cu(II)-O-O•$^-$ (**P$_{O2}$**; Supplementary Fig. 7) and celloheptaose-LPMO-Cu(II)-O-O•$^-$ (**P$_{O2}$-RH**; Supplementary Fig. 8) were tested and compared. Moreover, both side-on and end-on binding to yield **P$_{O2}$** were explored. The lowest energy state for **P$_{O2}$** was found to be the triplet state with the superoxide ion binding equatorially to copper in an end-on fashion, with O-O distance equal to 1.27Å. The electronic structure is compatible with a LPMO-Cu(II)-O_2^- description, according to the charges and spin populations. The singlet state was 10.6 kcal/mol higher in energy than the triplet one, and the O_2 binding energy to the LPMO-Cu(I) site was found to be -6.5 kcal/mol. The triplet-singlet energy difference is higher with respect to the value reported by Kjaergaard *et al.*[24] for their AA9 LPMO from *T. aurantiacus* (4.5 kcal/mol), whereas the O_2 binding energy reported in the same investigation is significantly lower (-0.7 kcal/mol). The binding of O_2 yields a distorted tetrahedral geometry of the Cu atom (see Fig. 2).

To investigate whether dioxygen binding to Cu(I) is assisted by the presence of a substrate molecule bound to the flat surface of the enzyme, we also optimized the geometry for the celloheptaose-LPMO-Cu(I) adduct (**P$_{RED}$-RH**) (i.e. in the absence of dioxygen), in order to compare the O_2 binding energy in the absence and in the presence of the substrate. We found that in the presence of the substrate, the O_2 binding is further favoured by 4.0 kcal/mol. In this case, the geometry of the Cu atom with bound dioxygen shows the same distorted tetrahedral geometry that was observed for **P$_{O2}$** without the substrate. Such distortion draws the Cu atom closer to the celloheptaose allowing the O_2 ligand to approach more closely the sugar. Interestingly, the energy difference in O_2 binding in absence and presence of celloheptaose is similar to that determined experimentally for the

14

binding of an oligosaccharide substrate in the presence and absence of chloride.[20] It is also worthy

of note that Cu(II) does not bind O_2, as the geometry optimization of the LPMO-Cu(II)-O_2 adduct

evolves by dissociating the O_2 ligand (see Supplementary Fig. 9). This finding confirms, as

observed experimentally, that Cu reduction is required for LPMO reactivity, and provides further

validation for the model and the level of the theory used here.

The Cu(II)-oxyl radical is responsible for hydrogen atom abstraction from the substrate

After formation of the superoxo $\mathbf{P_{O2}}$-**RH** species, different routes to substrate hydroxylation have

been hypothesized. Please note that, although the Nc-LPMO that we have investigated can oxidize

both the C1 and C4 positions of cellulose, in the present paper we only investigated the reaction

mechanism for C1. Although we cannot rule out differences between the oxidative mechanisms of

C1 and C4, previous DFT investigations showed that the oxidative mechanism at the two carbons is

most likely the same, with differences in the energy barriers as low as 2-4 kcal/mol.[26]

Once the superoxo species has been formed, there are several distinct proposed pathways that could

lead to substrate hydroxylation: they can be classified based on what is the reaction intermediate

that performs the HAA from the sugar carbon atom. In particular, three different classes of

mechanisms are investigated in this work (see Fig. 3). In the first class, that was proposed based on

the analogy with other copper-dependent monooxygenases, the superoxo intermediate itself

performs HAA on the substrate RH, forming a negatively charged Cu(II) hydroperoxo species and a

substrate radical R• (LPMO-Cu(II)-O-OH‾---•R). In the second group of proposed pathways, the

superoxo species is first protonated to give a O-OH group coordinated to copper that can perform

the HAA step. The third class of mechanisms is characterized by a double protonation of the

superoxo species, followed by the dissociation of a water molecule, resulting in a Cu(II)-oxyl

radical that perform the HAA step. These mechanisms may diverge, according to whether the

15

necessary electrons and protons are transferred separately or in combined steps, leading to different intermediate species. Another possible mechanism is based on the release of free superoxide ion right after the formation of the superoxo intermediate, that therefore acts as the ROS responsible for substrate hydroxylation. However, this mechanism is considered to be unlikely.[5,24] Indeed, it would lead to uncontrolled attack to the substrate, in contrast with experimental evidences,[50] especially concerning C1 and C4 regioselectivity, hinting at LPMOs acting via highly controlled reaction mechanisms.
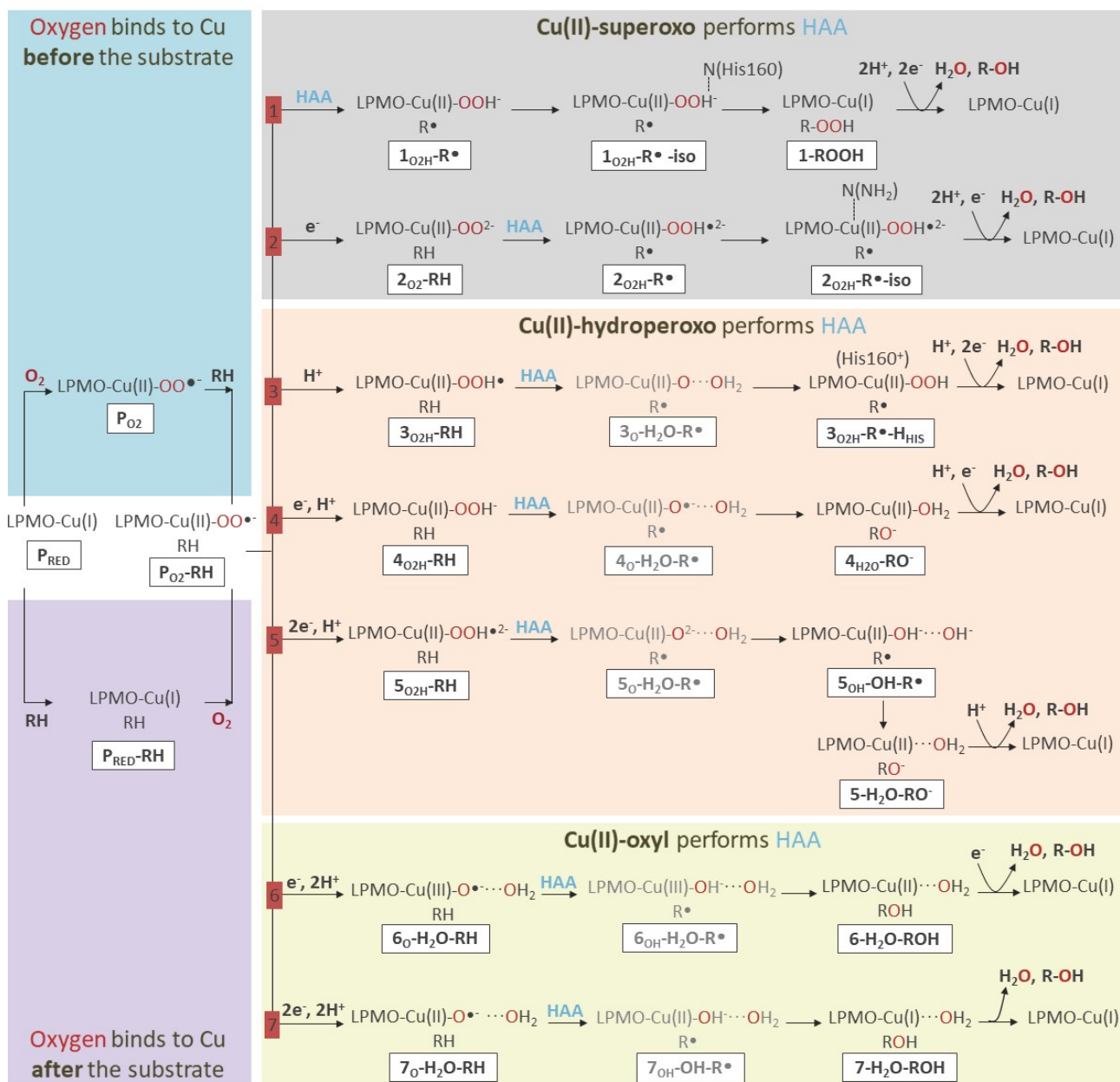
Figure 3: Overview of the possible catalytic pathways proposed so far for LPMOs on polysaccharidic substrates (RH). Blue HAA label identifies the Hydrogen Atom Abstraction (HAA) step. Starting from the reduced form of the enzyme, LPMO-Cu(I) (**P_RED**, far left), two alternative routes are possible, depending on whether dioxygen binding occurs before (blue box) or after (purple box) that of the substrate to the protein. Both pathways would lead to a superoxo intermediate, LPMO-Cu(II)-OO•⁻, in contact with the substrate RH (**P_O2-RH**). Three distinct sets of pathways have been proposed for the oxidation of the polysaccharide: mechanisms 1 and 2 (grey box) are based on HAA performed directly by the superoxo intermediate, mechanisms 3, 4 and 5 (red box) are based on HAA by a Cu(II)-hydroperoxo intermediate, while mechanisms 6 and 7 (yellow box) are based on HAA by a Cu(II)-oxyl intermediate. Several species are depicted in a lighter shade of grey to indicate that they were not isolated as stable intermediates in this work.

17

We first explored the viability of the superoxo class of possible mechanisms (paths 1 and 2 in Fig. 3, grey box), which are based on the assumption that the HAA is performed by the O_2 coordinated in P_{O2}-RH, or by the intermediate that is formed after its mono-electron reduction (2_{O2}-RH). In the former case, the singlet spin state of the resulting LPMO-Cu(II)-O-OH$^-$···•R intermediate (1_{O2H}-R•) is slightly more stable by only 0.7 kcal/mol than the triplet one. The calculated energy difference associated to the HAA step by P_{O2}-RH to give the 1_{O2H}-R• intermediate is equal to +25.1 kcal/mol, indicating that such mechanism is a highly unfavourable process. This value is slightly smaller than that calculated by Kim *et al.*[26] (+32.3 kcal/mol) obtained using a much smaller active site model and imposing many more constraints. In our model, this energy difference subsequently slightly decreases to +23.4 kcal/mol as the O_2H group moves towards the CuN_3 plane to give a distorted square planar arrangement and forming H-bonds with His160 and a water molecule (1_{O2H}-R•-iso).

We also calculate a very large energy difference (+30.9 kcal/mol) when the hydrogen abstraction is preceded by the mono-electron reduction of the enzyme (path 2) to give the LPMO-Cu(II)-O-OH•$^{2-}$···•R (2_{O2H}-R•) hydroperoxo species. As in the previous case, the O-OH group can subsequently move towards the CuN_3 plane to give a more stable distorted square planar arrangement (+20.6 kcal/mol), but here the amine dissociates from the Cu atom, as the Cu-N(NH2) distance increases up to 3.511 Å (2_{O2H}-R•-iso). We did not calculate the energy of the transition states TS for such hydrogen abstraction reactions, because our results imply that an activation energy of *more than* 30 kcal/mol is required to form the 1_{O2H}-R• or the 2_{O2H}-R• species: this finding *per se* would suggest that P_{O2}-RH and 2_{O2}-RH intermediates are likely not to be the ROS species that are responsible for HAA. In fact, despite the remarkable scarcity of kinetic measurements

involving LPMOs, 30 kcal/mol is a value remarkably larger than barriers for the rate determining steps of different LPMOs either published[5] or estimated by us from reported reaction rates (k_{obs}) obtained at different temperatures[5,18,51,52] ranging from about 6 to ca. 15 kcal/mol.

We also explicitly tested the recently proposed[5] pathway in which the HAA by the superoxide was suggested to be followed by a rapid superoxyl rebound to give a peroxylated substrate R-OOH (continuation of path 1 in Fig. 3). In this respect, our calculations show that the latter species LPMO-Cu(I)···H-O-O-R (**1-ROOH**) is a stable intermediate and its energy is lower by about 8 kcal/mol than that of the superoxo **P$_{O2}$-RH** species. Nevertheless, this mechanism must also proceed through the highly unfavourable HAA by **P$_{O2}$-RH**. We can therefore rule out the superoxo mechanisms 1 and 2 as possible descriptions of the LPMO9 reactivity.

The second class of mechanisms involves the protonation of the O_2 coordinated in **P$_{O2}$-RH** to give a Cu(II)-hydroperoxo intermediate, which should perform HAA from the substrate (paths 3, 4 and 5 in Fig. 3, red box) yielding the LPMO-Cu(II)-O-OH$_2$···•R species. Such intermediate should then dissociate a water molecule, forming a Cu(II)-oxyl species with the oxygen atom that can be then transferred to the radical substrate. The HAA can be promoted by the LPMO-Cu(II)-O-OH• (**3$_{O2H}$-RH**) species (path 3) as well as, after its mono and di-electron reduction, by the LPMO-Cu(II)-O-OH$^-$ (**4$_{O2H}$-RH**; path 4) and LPMO-Cu(II)-O-OH•$^{2-}$ (**5$_{O2H}$-RH**; path 5) species, respectively.

The singlet spin state in **3$_{O2H}$-RH** is more stable than the triplet one by about 3.5 kcal/mol. Interestingly, the hydroperoxide ligand is coordinated in the equatorial plane, in good agreement with the crystallographic structure recently reported by O'Dell *et al.*,[53] featuring a diatomic oxygenic species coordinated to the Cu atom. In particular, the Cu-O and O-O distances in **3$_{O2H}$-RH**, equal to 1.97 and 1.41 Å, closely match the experimental values (1.90±0.05 and 1.44±0.06 Å, respectively). The only significant difference between the calculated and the experimental structure

lies in the distance between the hydroxyl group of Tyr173 and the Cu atom that in the former (4.2 Å) is about 1.5 Å larger than in the latter (2.7 Å). In this respect, it is important to note that the experimental value indicates that Tyr is no longer coordinated to Cu, and significant fluctuations can therefore characterize the side chain of this residue. That might also arise from the fact that the Tyr is located at the edge of the active site model, and therefore might experience larger fluctuations than one would observe if the protein residues were taken into account. Nevertheless, since the Tyr is no longer bound to copper, such large fluctuations should not affect the electronic structure nor the energetics along the reaction pathways.

HAA by 3_{O2H}-**RH,** in which the hydrogen atom is transferred to the protonated oxygen of the O-OH group, does not lead to the dissociation of a water molecule but rather to a proton transfer from the O-OH$_2$ group to the Nδ atom of His160 (3_{O2H}-**R•-H$_{HIS}$**). This species is less stable than the reactant (3_{O2H}-**RH**) by as much as 28 kcal/mol, suggesting that also this pathway is unfavourable for LPMO9s. In addition, the peripheral oxygen atom that should bind the C4 hydrogen is at a distance of more than 3 Å from such hydrogen in the reactant. The oxygen atom coordinated to Cu, which is much closer (2.31Å) to the C4 hydrogen, may assist its transfer to the peripheral oxygen. However, the intermediate featuring the Cu-OH-OH coordination is about 36 kcal/mol less stable than the reactant.

Protonation of the superoxide in **P$_{O2}$-RH** coupled to a mono electron reduction gives the LPMO-Cu(II)-O-OH¯ (**4$_{O2H}$-RH**) doublet species (path 4). In this case, we can also evaluate the energetics of the coupled proton and electron transfer steps by using the ascorbic acid (**AA**) as reductant and proton donor agent (by its conversion to semidehydroascorbic acid, **SAA**). In fact, the process **P$_{O2}$-RH + AA → 4$_{O2H}$-RH + SAA** is slightly favourable by about 1 kcal/mol. In **4$_{O2H}$-RH,** the Cu atom is still in a pseudo square planar geometry. The unpaired electron is mainly localized on the Cu

atom, indicating that the O-OH group can be considered a hydroperoxide coordinated to a Cu(II) atom. Notably, the subsequent HAA by this species leads to the dissociation of a water molecule and the formation of a Cu(II)-oxyl species. The oxyl ligand of this intermediate moves spontaneously, during geometry optimization, to the radical carbon atom of the sugar through a rebound mechanism producing the alkoxide. The entire process is exoenergetic by as much as 59 kcal/mol. Interestingly, in the final product (4_{H2O}-RO⁻) the formed water molecule coordinates the Cu atom, which therefore preserves a pseudo square planar coordination mode. In this case, we were not able to characterize the TS to calculate the activation energy of the HHA step. However, our best TS guess structure (obtained by scanning the PES of the system along the reaction coordinate) is 30 kcal/mol higher in energy compared to the reactant. Although this is not a genuine energy barrier, such high value suggest that we can confidently rule out this pathway, at least for fungal LPMOs.

Two electron reduction and protonation of P_{O2}-RH leads to the LPMO-Cu(II)-O-OH^{2-} (5_{O2H}-RH) species, which can evolve similarly to 4_{O2H}-RH (path 5 in Fig. 3). The singlet state of 5_{O2H}-RH is more stable than the triplet one by 20.4 kcal/mol. 5_{O2H}-RH can abstract the hydrogen atom of the sugar leading to the formation of a water molecule that dissociates from the metal. Interestingly, during geometry optimization one H atom of the water molecule moves to the oxyl group to give an OH group coordinated to the Cu atom and leaving a hydroxide ion which forms a H-bond with such hydroxyl group. This species (5_{OH}-OH-R•) can be isolated as a stable intermediate and it is about 2 kcal/mol more stable than the reactant (5_{O2H}-RH). The hydroxyl group of 5_{OH}-OH-R• can then move to the radical carbon atom of the sugar through a rebound mechanism to give the alcohol and a tricoordinated Cu(I) complex. It is worth noting that after the formation of the product, the proton of the alcoholic function moves to the hydroxide ion with the final formation of a water molecule and the alkoxide. This product (5-H$_2$O-RO⁻) is about 83 kcal/mol more stable than the 5_{OH}-OH-R•

21

intermediate. Similarly to what we had just described for path 4, we could not localize the TS to calculate the activation energy of the HHA step, although the very high energy (32 kcal/mol) of our best TS guess allows us to rule out this mechanism as well.

The third group of mechanisms is based on the assumption that a Cu(II)-oxyl species is instead the ROS that abstracts a hydrogen atom from the sugar substrate. Also in this case, two different paths are possible, depending on whether a mono- or dielectronic reduction precedes the HAA step (paths 6 and 7, respectively, in Fig. 3, yellow box). We first tested mechanism 6, where two protons and one electron are transferred to the active site leading to the formation of a Cu(III)-O•¯ oxyl radical species or its resonance form Tyr171($\bullet^+$)--Cu(II)-O•¯ oxyl, with the concomitant release of a water molecule. In fact, when a second proton is added to the doublet Cu(II)-hydroperoxo intermediate $\mathbf{4_{O2H}\text{-}RH}$, geometry optimization leads to the species $\mathbf{6_O\text{-}H_2O\text{-}RH}$, in which a water molecule dissociates, remaining in close proximity of the active site upon formation of a H-bond interaction with the oxyl group. The spin state of $\mathbf{6_O\text{-}H_2O\text{-}RH}$ was investigated by calculating the quartet state (S=3/2) and the two BS doublet states (S=1/2) with the 'net unpaired' electron either initially localized on the Cu-oxyl moiety or the Tyr residue. It turned out that the last spin configuration is more stable than the other two by about 2 kcal/mol (these two spin configurations are basically isoenergetic). Analysis of charge and spin populations show that in the most stable spin state the aromatic ring of Tyr171 possess a significant radical and cationic character, whereas the net spin density on the Cu-O moiety is negligible, indicating that the electronic structure of $\mathbf{6_O\text{-}H_2O\text{-}RH}$ can be better represented as Tyr171($\bullet^+$)--Cu(II)-O•¯ rather than Tyr171--Cu(III)-O•¯. The Cu-O distance in $\mathbf{6_O\text{-}H_2O\text{-}RH}$ is equal to 1.80Å and the oxygen atom is slightly out of the CuN₃O square plane by approaching the hydrogen atom of C4 at a distance of only 2Å. Indeed, the oxyl ROS can easily abstract the H atom from the sugar leading to the hydroxyl intermediate LPMO-Cu(II)-OH¯, which, at variance with the previously proposed mechanism,[26] cannot be isolated as a stable

intermediate (see Supplementary Fig. 10). In our calculations, the LPMO-Cu(II)-OH$^-$ species spontaneously evolves with migration of the •OH hydroxyl from the Cu atom to the radical carbon atom of the sugar, to give the hydroxylated substrate R-OH (**6-H$_2$O-ROH**). The product is about 57 kcal/mol lower in energy than **6$_O$-H$_2$O-RH** and regenerates the LPMO-Cu(II) form of the enzyme. Notably, the calculated energy barrier of the HAA step, equal to 14.8 kcal/mol (8.1 kcal/mol for the small model; see Fig. 4a and Supplementary Fig. 11), is sufficiently small to support the reliability of this mechanism. It should also be noted that the H-abstraction from the oxyl radical species and the subsequent hydroxyl rearrangement is similar to the mechanism proposed for the oxidation of CH$_4$ to CH$_3$OH catalysed by methane monooxygenase.[54] An essential feature of the proposed mechanism is the pivotal role of the water molecule, dissociated from the copper coordination sphere, in assisting both the Cu-OH bond cleavage first and then the formation of the new R-OH bond. This essential role played by such water molecule can be visualized in the attached Supplementary Video 1 (please see also Supplementary Fig. 10).

We also investigated the mechanism assuming that HAA occurs after a dielectronic reduction of the the Cu(II)-superoxo intermediate with the concomitant addition of two protons (path 7). The energetics of the coupled addition of the second proton and electron to **4$_{O2H}$-RH** can also be evaluated by considering the semidehydroascorbic (**SAA**) acid as reductant to give the dehydroascorbic acid (**DHAA**). In this case, the reaction **4$_{O2H}$-RH + SAA → 7$_O$-H$_2$O-RH + DHAA** is exoenergetic by about 34 kcal/mol. For this intermediate (**7$_O$-H$_2$O-RH)** the BS S=0 and the S=1 spin states are almost (within 0.2 kcal/mol) isoenergetic. We found that the reaction can occur with a mechanism very similar to that discussed above. Also in this case, the oxyl radical species can easily abstract the hydrogen atom from the substrate and the formed hydroxyl species coordinated to Cu spontaneously migrates to the radical carbon atom through a rebound mechanism. It should be noted that the geometry optimization of the barrierless hydroxyl rebound

has been carried out starting from a singlet BS spin state, in which the two opposite spins were localized on C1 and Cu, respectively. The BS solution then converged to a pure S=0 spin state, after several geometry optimization cycles. The product (**7-H$_2$O-ROH**) is 53.9 kcal/mol lower in energy than **7$_O$-H$_2$O-RH** and regenerates the LPMO-Cu(I) form of the enzyme. Although in the product the metal atom is in the Cu(I) redox state, it features a geometry very similar to that of the corresponding Cu(II) species (see Fig. 4c). More importantly, the energy barrier to the TS of this reaction mechanism is equal to 6.2 kcal/mol (3.6 kcal/mol for the small model; see Fig. 4a and Supplementary Fig. 11), a value further lower than the barrier calculated for mechanism 6 (14.8 kcal/mol) indicating that, among all the investigated LPMO9s pathways, this is the more reliable.
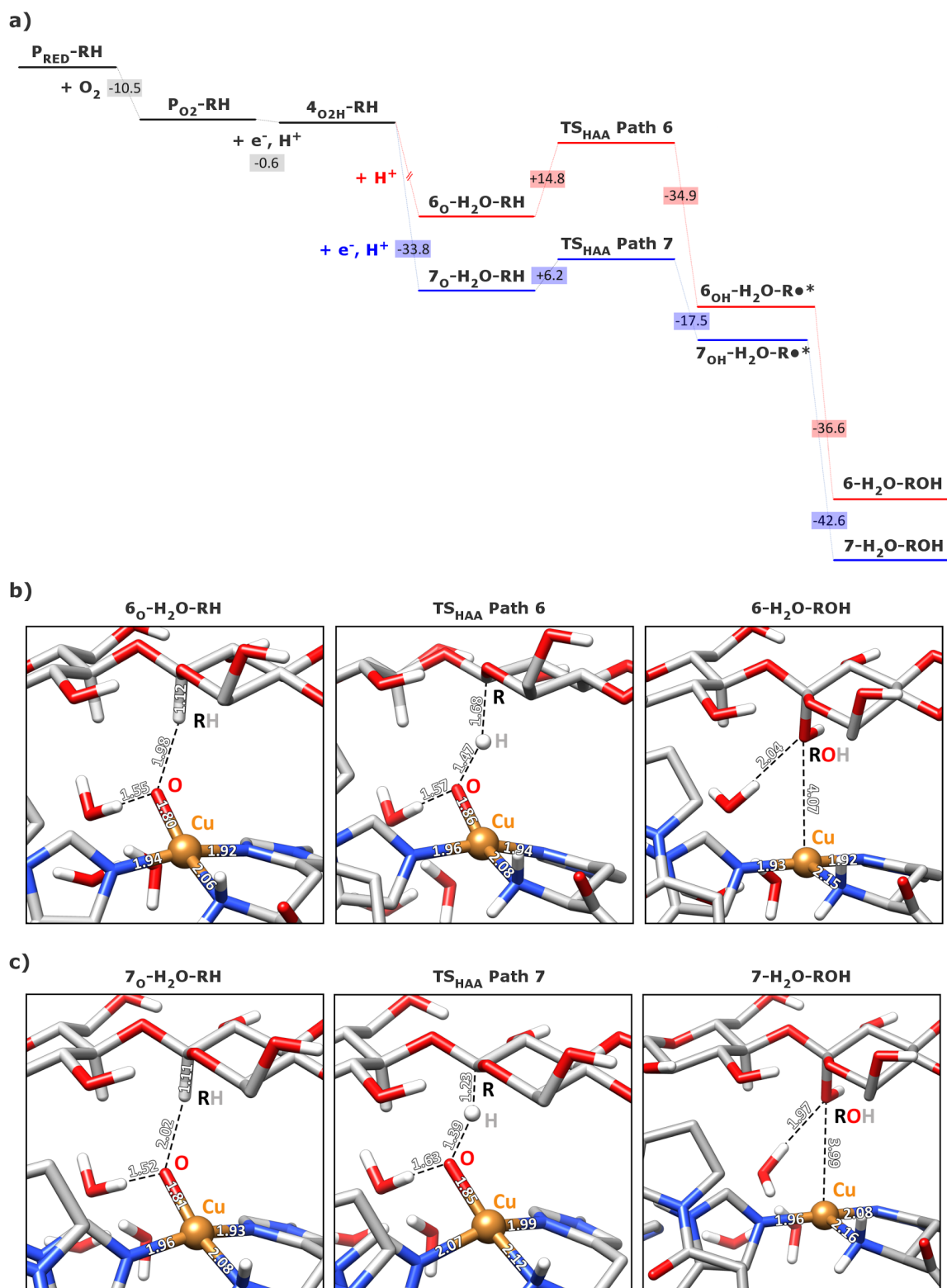
Figure 4. (a) Potential energy diagram for the most plausible pathways for the LPMO catalytic mechanism; red and blue lines indicate reaction steps involved in Paths 6 and 7, respectively. It is worth noting that the energy of **6$_{OH}$-H$_2$O-R•** and **7$_{OH}$-H$_2$O-R•**, marked with an asterisk in the

25

figure, has been estimated from the geometry optimization of their structures before the hydroxyl group migrates from the Cu atom to the substrate to yield the hydroxylated product R-OH (see Fig. 10 in SI). The energy values for the initial reactants, the transition states and the final products are expressed in kcal/mol. DFT optimized structures of the stable intermediates identified along Paths 6 and 7 are shown in panels (b) and (c), respectively. For the sake of clarity, aliphatic hydrogen atoms (with exception of hydrogen atoms of C1 and C4) are not shown. Selected distances are given in Å.

The formation of the Cu(II)-O$^-$ oxyl intermediate can be followed by a proton transfer from the terminal amino group coordinated to the Cu atom to the oxyl oxygen atom to give the Cu(III)-OH tautomer, as recently observed in mononuclear copper model complexes.[55,56] In fact, the transfer of a proton from the NH_2 group of His1 to the Cu(II)-O$^-$• oxyl to give the **7$_{OH-NH}$-H$_2$O-RH** species is energetically favoured by 11.7 kcal/mol. However, **7$_{OH-NH}$-H$_2$O-RH** is 42.4 kcal/mol less stable than the isomer obtained by HAA on the substrate **7-H$_2$O-ROH**, suggesting that the latter process (also considering the small activation barrier) is to be preferred with respect to the former. Nevertheless, the Cu(III)-OH tautomer can be formed to stabilize the reactive Cu(II)-O$^-$• oxyl intermediate if HAA reaction does not occur very quickly. Cu(III)-OH can then be the species responsible for the HAA on the substrate according to the mechanism proposed for a mononuclear copper model complex.[55,56]

Very recently H_2O_2, rather than O_2, has been proposed as the 'catalytically relevant co-substrate' oxidant in the cellulose hydroxylation.[23] H_2O_2 has the advantage, with respect to O_2, that no additional protons and electrons are required for the reaction to occur, even if its occurrence in the reaction environment is debatable. In the proposed mechanism, the binding of H_2O_2 to the active site should be followed by an intramolecular proton transfer from the coordinated to the distal oxygen atom of H_2O_2 and the dissociation of a water molecule. This yields the Cu(II)-oxyl intermediate, corresponding to the **7$_O$-H$_2$O-RH** species. The reaction can then proceed following

the path 7 discussed above. Prompted by the study of Bissaro *et al.*,[23] we have performed a preliminary investigation of the binding of H_2O_2 to the LPMO-Cu(I) active site of $\mathbf{P_{RED}}$. We found that H_2O_2 can indeed coordinate to the Cu atom in the equatorial plane yielding a slightly distorted square planar geometry. The binding energy for the formation of the $\mathbf{P_{RED}}$-H_2O_2 adduct ($\mathbf{P_{H2O2}}$) from $\mathbf{P_{RED}}$ is equal to about -4 kcal/mol. The coordination of H_2O_2 in $\mathbf{P_{H2O2}}$ is almost linear, with the Cu-O-O angle equal to 169°, and the Cu-O and O-O distances equal to 2.50 and 1.56 Å, respectively. This result suggests that oxidation of the substrate by H_2O_2 is a reliable process, as the binding of H_2O_2 in the presence of the substrate may led to the Cu(II)-oxyl intermediate.

DISCUSSION

The recent crystal structure of an LPMO-polysaccharide complex shows the formation of a cavity at the LPMO active site upon substrate binding.[20] This event raises the possibility that the interaction between the enzyme and the polysaccharide controls the affinity of O_2 for LPMO.[5] Our calculations support this hypothesis: in fact, we observe a 4.0 kcal/mol stabilization of the O_2 binding to Cu induced by the presence of bound substrate. This energy difference is not large enough to let us infer that O_2 can bind to LPMO *only* in the presence of a substrate. Nevertheless, it provides further evidence for a mutually dependent binding of dioxygen and polysaccharide. This might serve as a substrate-controlled protective mechanism of fungal LPMOs against uncontrolled generation of ROS[5,13,57] such as hydroxyl radicals. These radicals might on one side enhance direct non-enzymatic degradation of lignocellulose, but on the other lead to undesired inactivation of many other enzymes and of the LPMO itself.

Moreover, by inspection of the various optimized structures presented here, it is possible to tentatively assign some amino acids beyond the first copper coordination sphere a role in assisting

the catalytic mechanism. In particular, Trp78 is found in all structures to warrant proper orientation of the Tyr171 hydroxyl group toward the copper atom. This is achieved thanks to a stacking interaction involving the indole and phenyl ring planes, which are perpendicular to each other, preventing Tyr171 fluctuations. We also assign a major role to Gln169 and His160 in the reaction mechanism: in our optimized structure, both residues keep the water molecule that leaves the first coordination sphere upon Cu reduction close to the active site. The presence of that water molecule is crucial to the catalytic mechanism, since it allows for the hydroxyl rebound that generates the final product. Moreover, Gln169 and His160 belong to a highly conserved H-bonds motif in LPMOs and the assigned role in assisting the LPMO reactivity is in line with recent experimental findings.[48] EPR spectroscopy experiments by Span *et al.* suggests that they are involved in stabilizing the coordinated superoxide ion,[48] but the spacer region that separates the conserved His and Gln is exceptionally shorter in the LPMO they investigated (5 residues) than in most of other LPMOs, as the one that we are modelling here (8 residue-long loop).

Besides showing the synergistic nature of substrate-dioxygen binding to LPMO9s, the present results address the question of the identity of the species responsible for HAA on the substrate, that turns out to be a Cu(II)-oxyl intermediate. We therefore confirm previous computational[26] and experimental[48] studies that suggest Cu(II)-oxyl-based mechanism for LPMO catalytic activity. Nevertheless, when compared to the results by Kim *et al.*,[26] we calculate significantly lower activation barriers and our mechanism further differs, since here the hydroxyl intermediate LPMO-Cu(II)-OH⁻ could not be isolated, with the -OH group spontaneously migrating to bind to the radical carbon of the polysaccharide, with a water assisted rebound step (see Supplementary Video 1).

The very high energy difference calculated for the superoxo species apparently rules out the

mechanisms based on abstraction of a hydrogen atom from the substrate by the Cu(II)-O-O$^{\bullet-}$ and Cu(II)-O-O^{2-} moiety itself. This is in agreement with recent experimental investigations, where the results of EPR and activity essays on a fungal LPMO indicated that the Cu(II)-superoxo is not the active species in the catalytic mechanism.[48] We have also investigated hydroperoxo-based mechanisms, which, despite being overall exoenergetic, are disfavored by the high (30 kcal/mol or more) estimated barriers.

The role of the Cu(II)-oxyl is similar to that of the oxy-ferryl intermediate in P450 monooxygenases, the most widely studied example of C-H oxygenation, although occurring at an heme iron center.[12] Admittedly, the Cu(II)-oxyl species has not been experimentally observed yet and doubts were raised[5] on the involvement of such a high valent intermediate with potentially significant oxidizing ability in the LPMO mechanism. Yet, we find the Cu(II)-oxyl species to be stable and we calculate an activation barrier as low as 6.2 kcal/mol that allows Cu(II)-oxyl to perform quasi-barrierless HAA, in line with previous predictions.[26]

It might be possible that the present mechanism is applicable to fungal LPMOs only. In fact, while cellobiose dehydrogenase (CDH) is most likely the 2-electron donor required in the reaction path described here for AA9,[58] AA11 and AA13, a redox partner fulfilling the same role has yet to be identified for AA10 LPMOs. Recently,[58] fungal LPMOs were found to be very versatile in being reduced by extracellular electron donors others than CDH, such as plant-derived phenolic compounds, which can also serve as mediators for glucose-methanol-choline (GMC) oxidoreductases. The calculated values for the TS of the two possible Cu(II)-oxyl-based catalytic pathways suggest that the two electrons that are required for the monooxygenation reaction enter the active site simultaneously (pathway 7 in Fig. 3) rather than in two separate steps (pathway 6 in Fig. 3). Simple charge-based arguments would suggest concerted transfer of H$^+$ and electrons, since

this avoids energetically demanding transfer of one net positive charge. Therefore, in our proposed mechanism, the starting and final state of the catalytic cycle is LPMO-Cu(I), without passing through a LPMO-Cu(II) intermediate. Although the E^0 for the particular LPMO investigated here is not known, reduction potentials of other LPMOs from fungi and bacteria have been reported.[9,18,59] The E^0 values fall in the 224-275 mV (vs SHE) range. Such a positive reduction potential indicates that, in these species, the reduced Cu(I) state is rather stable. It is likely that, in the absence of substrate, the Cu(II) state might be stabilized over Cu(I) as a consequence of the higher exposure of the active site to the solvent. This would prevent O_2 binding to the LPMO active site in the absence of polysaccharide, since oxidized Cu is known to have very low affinity for dioxygen.[60]

For the above, we propose the following LPMO9 mechanism, as depicted in Fig. 5: the inactive form of the enzyme is LPMO-Cu(II), with no affinity for molecular oxygen (state 0); a one-electron reduction process activates the protein to LPMO-Cu(I) (state 1), which synergistically binds oxygen and the substrate to yield the superoxide intermediate (state 2). The LPMO then performs its catalytic cycle via two proton coupled electron transfer steps, leading to elimination of a water molecule and formation of a stable LPMO-Cu(II)-oxyl intermediate (consequential formation of state 3 and state 4). The latter abstracts a H atom from the C4 atom of the saccharide with a rapid, water assisted hydroxyl rebound to the substrate, leading to the formation of the product R-OH and regenerating the enzyme active form state LPMO-Cu(I). It might then be possible, as proposed elsewhere,[5] that the enzyme performs its catalytic activity while remaining attached to the polysaccharide surface, most likely processing along it to start a new catalytic cycle. Our calculations do not allow for any hypotheses to be put forward in this respect. Our results also show that H_2O_2 may replace O_2 as oxidant, because it binds to the active site and may yield the Cu(II)-oxyl intermediate after an intramolecular proton transfer and dissociation of a water molecule, without the requirement of additional electrons and protons. It is important to note that

our result do not demonstrate that H_2O_2 is the 'catalytically relevant co-substrate' in the cellulose hydroxylation, since other conditions, such as the accessibility of H_2O_2 to the active site, and its availability in the reaction environment should be considered.
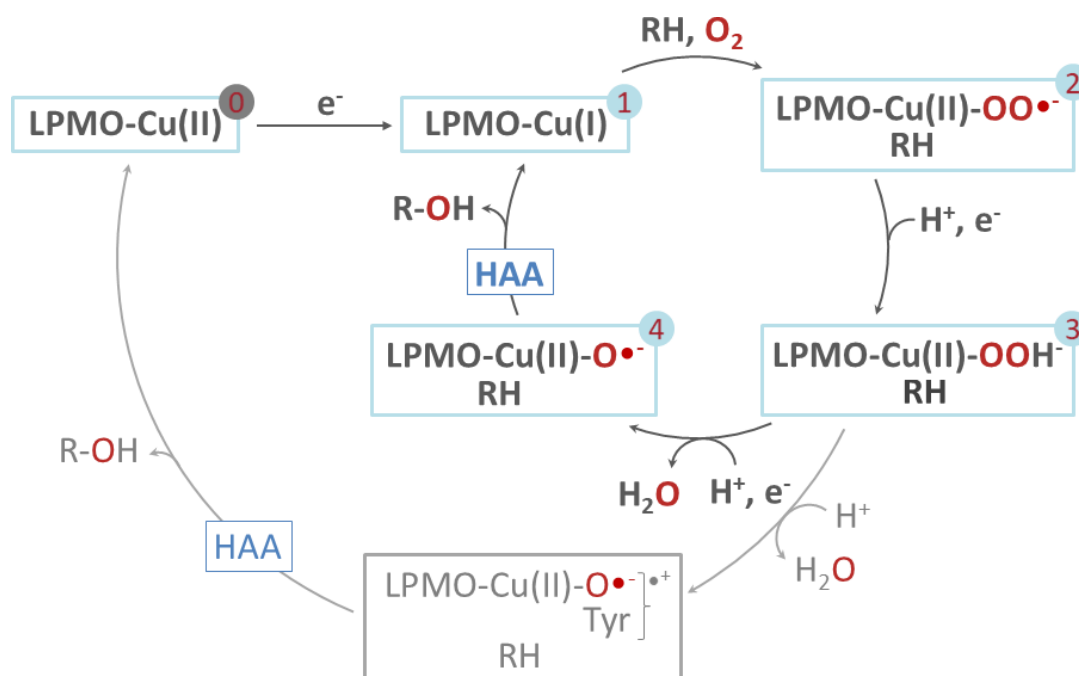

Figure 5. Schematic summary of the proposed mechanism of action of the investigated LPMOs, based on HAA performed by a Cu(II)-oxyl intermediate after a two proton coupled electron transfer (black arrows). The higher barrier mechanism involving two separate electron transfer steps is also shown (grey arrows).

In conclusion, we have applied DFT calculations to gain new insights into the catalytic mechanism of action of a fungal LPMO. The use of a very large active site model with a minimal number of constraints and the good agreement with published structural and computational data on this enzyme superfamily contribute to the high reliability of our predictions. Nevertheless, further experimental evidences, e.g. the determination of the redox potential via direct electrochemistry both for freely diffusing and substrate-bound enzyme, will help understanding whether the reaction pathway proposed here is exclusive to fungal species or can be extended to all LPMOs families.

Our results will help both the design of novel routes to copper-based oxygenase chemistry and the rational optimization of the use of these enzymes in the degradation of recalcitrant lignocellulosic substrates, a significant step towards the use of non-edible biomass as sustainable carbon source.

ACKNOWLEDGEMENTS

ADDITIONAL INFORMATION

Supplementary information regarding the details of the active site models, the electronic structure properties and the structural details of all the species identified along the investigated pathways are available in the online version of the paper.

REFERENCES

(1)   Beeson, W. T.; Vu, V. V.; Span, E. A.; Phillips, C. M.; Marletta, M. A. Cellulose Degradation by Polysaccharide Monooxygenases. *Annu. Rev. Biochem.* **2014**, *84* (1), 150317182619002 DOI: 10.1146/annurev-biochem-060614-034439.

(2)   Lo Leggio, L.; Simmons, T. J.; Poulsen, J.-C. N.; Frandsen, K. E. H.; Hemsworth, G. R.; Stringer, M. A.; von Freiesleben, P.; Tovborg, M.; Johansen, K. S.; De Maria, L.; Harris, P. V; Soong, C.-L.; Dupree, P.; Tryfona, T.; Lenfant, N.; Henrissat, B.; Davies, G. J.; Walton, P. H. Structure and Boosting Activity of a Starch-Degrading Lytic Polysaccharide Monooxygenase. *Nat. Commun.* **2015**, *6*, 5961 DOI: 10.1038/ncomms6961.

(3)   Span, E. A.; Marletta, M. A. The Framework of Polysaccharide Monooxygenase Structure and Chemistry. *Curr. Opin. Struct. Biol.* **2015**, *35*, 93–99 DOI: 10.1016/j.sbi.2015.10.002.

(4)   Hemsworth, G. R.; Johnston, E. M.; Davies, G. J.; Walton, P. H. Lytic Polysaccharide

        Monooxygenases in Biomass Conversion. *Trends Biotechnol.* **2015**, *33* (12), 747–761 DOI:

        10.1016/j.tibtech.2015.09.006.

(5)   Walton, P. H.; Davies, G. J. On the Catalytic Mechanisms of Lytic Polysaccharide

        Monooxygenases. *Curr. Opin. Chem. Biol.* **2016**, 1–13 DOI: 10.1016/j.cbpa.2016.04.001.

(6)   Isaksen, T.; Westereng, B.; Aachmann, F. L.; Agger, J. W.; Kracher, D.; Kittl, R.; Ludwig,

        R.; Haltrich, D.; Eijsink, V. G. H.; Horn, S. J. A C4-Oxidizing Lytic Polysaccharide

        Monooxygenase Cleaving Both Cellulose and Cello-Oligosaccharides. *J. Biol. Chem.* **2014**,

        289 (5), 2632–2642 DOI: 10.1074/jbc.M113.530196.

(7)   Arfi, Y.; Shamshoum, M.; Rogachev, I.; Peleg, Y.; Bayer, E. A. Integration of Bacterial

        Lytic Polysaccharide Monooxygenases into Designer Cellulosomes Promotes Enhanced

        Cellulose Degradation. *Proc. Natl. Acad. Sci.* **2014**, *111* (25), 9109–9114 DOI:

        10.1073/pnas.1404148111.

(8)   Busk, P. K.; Lange, L. Classification of Fungal and Bacterial Lytic Polysaccharide

        Monooxygenases. *BMC Genomics* **2015**, *16* (1), 368 DOI: 10.1186/s12864-015-1601-6.

(9)   Forsberg, Z.; Mackenzie, A. K.; Sørlie, M.; Røhr, Å. K.; Helland, R.; Arvai, A. S.; Vaaje-

        Kolstad, G.; Eijsink, V. G. H. Structural and Functional Characterization of a Conserved Pair

        of Bacterial Cellulose-Oxidizing Lytic Polysaccharide Monooxygenases. *Proc. Natl. Acad.

        Sci. U. S. A.* **2014**, *111* (23), 8446–8451 DOI: 10.1073/pnas.1402771111.

(10)   Hemsworth, G. R.; Taylor, E. J.; Kim, R. Q.; Gregory, R. C.; Lewis, S. J.; Turkenburg, J. P.;

        Parkin, A.; Davies, G. J.; Walton, P. H. The Copper Active Site of CBM33 Polysaccharide

        Oxygenases. *J. Am. Chem. Soc.* **2013**, *135* (16), 6069–6077 DOI: 10.1021/ja402106e.

(11)   Hemsworth, G. R.; Henrissat, B.; Davies, G. J.; Walton, P. H. Discovery and

        Characterization of a New Family of Lytic Polysaccharide Monooxygenases. *Nat. Chem.*

Biol. **2013**, *10* (2), 122–126 DOI: 10.1038/nchembio.1417.

(12)   Lee, J. Y.; Karlin, K. D. Elaboration of Copper-Oxygen Mediated CH Activation Chemistry

in Consideration of Future Fuel and Feedstock Generation. *Curr. Opin. Chem. Biol.* **2015**,

25, 184–193 DOI: 10.1016/j.cbpa.2015.02.014.

(13)   Johansen, K. S. Lytic Polysaccharide Monooxygenases: The Microbial Power Tool for

Lignocellulose Degradation. *Trends Plant Sci.* **2016**, *21* (11), 926–936 DOI:

10.1016/j.tplants.2016.07.012.

(14)   Harris, P. V.; Xu, F.; Kreel, N. E.; Kang, C.; Fukuyama, S. New Enzyme Insights Drive

Advances in Commercial Ethanol Production. *Curr. Opin. Chem. Biol.* **2014**, *19* (1), 162–

170 DOI: 10.1016/j.cbpa.2014.02.015.

(15)   Levasseur, A.; Drula, E.; Lombard, V.; Coutinho, P. M.; Henrissat, B. Expansion of the

Enzymatic Repertoire of the CAZy Database to Integrate Auxiliary Redox Enzymes.

Biotechnol. Biofuels **2013**, *6* (1), 1–14 DOI: 10.1186/1754-6834-6-41.

(16)   Wu, M.; Beckham, G. T.; Larsson, A. M.; Ishida, T.; Kim, S.; Payne, C. M.; Himmel, M. E.;

Crowley, M. F.; Horn, S. J.; Westereng, B.; Igarashi, K.; Samejima, M.; Ståhlberg, J.;

Eijsink, V. G. H.; Sandgren, M. Crystal Structure and Computational Characterization of the

Lytic Polysaccharide Monooxygenase GH61D from the Basidiomycota Fungus

Phanerochaete Chrysosporium. *J. Biol. Chem.* **2013**, *288* (18), 12828–12839 DOI:

10.1074/jbc.M113.459396.

(17)   Vu, V. V.; Beeson, W. T.; Phillips, C. M.; Cate, J. H. D.; Marletta, M. A. Determinants of

Regioselective Hydroxylation in the Fungal Polysaccharide Monooxygenases. *J. Am. Chem.*

Soc. **2014**, *136* (2), 562–565 DOI: 10.1021/ja409384b.

(18)   Borisova, A. S.; Isaksen, T.; Dimarogona, M.; Kognole, A. A.; Mathiesen, G.; Várnai, A.;

Røhr, Å. K.; Payne, C. M.; Sørlie, M.; Sandgren, M.; Eijsink, V. G. H. Structural and

Functional Characterization of a Lytic Polysaccharide Monooxygenase with Broad Substrate Specificity. *J. Biol. Chem.* **2015**, *290* (38), 22955–22969 DOI: 10.1074/jbc.M115.660183.

(19)   Vaaje-Kolstad, G.; Forsberg, Z.; Loose, J. S. M.; Bissaro, B.; Eijsink, V. G. H. Structural Diversity of Lytic Polysaccharide Monooxygenases. *Curr. Opin. Struct. Biol.* **2017**, *44*, 67–76 DOI: 10.1016/j.sbi.2016.12.012.

(20)   Frandsen, K. E. H.; Simmons, T. J.; Dupree, P.; Poulsen, J.-C. N.; Hemsworth, G. R.; Ciano, L.; Johnston, E. M.; Tovborg, M.; Johansen, K. S.; von Freiesleben, P.; Marmuse, L.; Fort, S.; Cottaz, S.; Driguez, H.; Henrissat, B.; Lenfant, N.; Tuna, F.; Baldansuren, A.; Davies, G. J.; Lo Leggio, L.; Walton, P. H. The Molecular Basis of Polysaccharide Cleavage by Lytic Polysaccharide Monooxygenases. *Nat. Chem. Biol.* **2016**, *12*, 298–303 DOI: 10.1038/nchembio.2029.

(21)   Courtade, G.; Wimmer, R.; Røhr, Å. K.; Preims, M.; Felice, A. K. G.; Dimarogona, M.; Vaaje-kolstad, G.; Sørlie, M.; Sandgren, M.; Ludwig, R.; Eijsink, V. G. H. Interactions of a Fungal Lytic Polysaccharide Monooxygenase with β -Glucan Substrates and Cellobiose Dehydrogenase. *Proc Natl Acad Sci U S A* **2016**, *113* (21), 5922–5927 DOI: 10.1073/pnas.1602566113.

(22)   Vaaje-Kolstad, G.; Westereng, B.; Horn, S. J.; Liu, Z.; Zhai, H.; Sorlie, M.; Eijsink, V. G. H. An Oxidative Enzyme Boosting the Enzymatic Conversion of Recalcitrant Polysaccharides. *Science (80-.).* **2010**, *330*, 219–222 DOI: 10.1126/science.1192231.

(23)   Bissaro, B.; Røhr, Å. K.; Müller, G.; Chylenski, P.; Skaugen, M.; Forsberg, Z.; Horn, S. J.; Vaaje-Kolstad, G.; Eijsink, V. G. H. Oxidative Cleavage of Polysaccharides by Monocopper Enzymes Depends on H2O2. *Nat. Chem. Biol.* **2017**, *13* (10), 1123–1128 DOI: 10.1038/nchembio.2470.

(24)   Kjaergaard, C. H.; Qayyum, M. F.; Wong, S. D.; Xu, F.; Hemsworth, G. R.; Walton, D. J.;

Young, N. a; Davies, G. J.; Walton, P. H.; Johansen, K. S.; Hodgson, K. O.; Hedman, B.; Solomon, E. I. Spectroscopic and Computational Insight into the Activation of O2 by the Mononuclear Cu Center in Polysaccharide Monooxygenases. *Proc. Natl. Acad. Sci. U. S. A.* **2014**, *111* (24), 8797–8802 DOI: 10.1073/pnas.1408115111.

(25) Li, X.; Beeson, W. T.; Phillips, C. M.; Marletta, M. a; Cate, J. H. D. Structural Basis for Substrate Targeting and Catalysis by Fungal Polysaccharide Monooxygenases. *Structure* **2012**, *20* (6), 1051–1061 DOI: 10.1016/j.str.2012.04.002.

(26) Kim, S.; Ståhlberg, J.; Sandgren, M.; Paton, R. S.; Beckham, G. T. *Quantum Mechanical Calculations Suggest That Lytic Polysaccharide Monooxygenases Use a Copper-Oxyl, Oxygen-Rebound Mechanism.*; 2014; Vol. 111.

(27) Horn, S. J.; Vaaje-Kolstad, G.; Westereng, B.; Eijsink, V. G. Novel Enzymes for the Degradation of Cellulose. *Biotechnol. Biofuels* **2012**, *5* (1), 45 DOI: 10.1186/1754-6834-5-45.

(28) Bruschi, M.; Tiberti, M.; Guerra, A.; De Gioia, L. Disclosure of Key Stereoelectronic Factors for Efficient H2 Binding and Cleavage in the Active Site of [NiFe]-Hydrogenases. *J. Am. Chem. Soc.* **2014**, *136* (5), 1803–1814 DOI: 10.1021/ja408511y.

(29) Himo, F. Recent Trends in Quantum Chemical Modeling of Enzymatic Reactions. *J. Am. Chem. Soc.* **2017**, *139* (20), 6780–6786 DOI: 10.1021/jacs.7b02671.

(30) Siegbahn, P. E. M.; Himo, F. The Quantum Chemical Cluster Approach for Modeling Enzyme Reactions. *Wiley Interdiscip. Rev. Comput. Mol. Sci.* **2011**, *1* (3), 323–336 DOI: 10.1002/wcms.13.

(31) Siegbahn, P. E. M.; Himo, F. Recent Developments of the Quantum Chemical Cluster Approach for Modeling Enzyme Reactions. *JBIC J. Biol. Inorg. Chem.* **2009**, *14* (5), 643–651 DOI: 10.1007/s00775-009-0511-y.

(32) Becke, A. D. Density-Functional Exchange-Energy Approximation with Correct Asymptotic Behavior. *Phys. Rev. A* **1988**, *38* (6), 3098–3100 DOI: 10.1103/PhysRevA.38.3098.

(33) Perdew, J. P. Density-Functional Approximation for the Correlation Energy of the Inhomogeneous Electron Gas. *Phys. Rev. B* **1986**, *33* (12), 8822–8824 DOI: 10.1103/PhysRevB.33.8822.

(34) Schäfer, A.; Huber, C.; Ahlrichs, R. Fully Optimized Contracted Gaussian Basis Sets of Triple Zeta Valence Quality for Atoms Li to Kr. *J. Chem. Phys.* **1994**, *100* (8).

(35) Eichkorn, K.; Weigend, F.; Treutler, O.; Ahlrichs, R. Auxiliary Basis Sets for Main Row Atoms and Transition Metals and Their Use to Approximate Coulomb Potentials. *Theor. Chem. Acc.* **1997**, *97* (1), 119–124 DOI: 10.1007/s002140050244.

(36) Ahlrichs, R.; Bär, M.; Häser, M.; Horn, H.; Kölmel, C. Electronic Structure Calculations on Workstation Computers: The Program System Turbomole. *Chem. Phys. Lett.* **1989**, *162* (3), 165–169 DOI: http://dx.doi.org/10.1016/0009-2614(89)85118-8.

(37) Prosdocimi, T.; De Gioia, L.; Zampella, G.; Bertini, L. On the Generation of OH· Radical Species from H2O2 by Cu(I) Amyloid Beta Peptide Model Complexes: A DFT Investigation. *J. Biol. Inorg. Chem.* **2016**, *21* (2), 197–212 DOI: 10.1007/s00775-015-1322-y.

(38) Bertini, L.; Bruschi, M.; Romaniello, M.; Zampella, G.; Tiberti, M.; Barbieri, V.; Greco, C.; La Mendola, D.; Bonomo, R. P.; Fantucci, P.; De Gioia, L. Copper Coordination to the Putative Cell Binding Site of Angiogenin: A DFT Investigation. *Theor. Chem. Acc.* **2012**, *131* (3), 1186 DOI: 10.1007/s00214-012-1186-y.

(39) Noodleman, L. Valence Bond Description of Antiferromagnetic Coupling in Transition Metal Dimers. *J. Chem. Phys.* **1981**, *74* (10).

(40) Noodleman, L.; Norman, J. G. The Xα Valence Bond Theory of Weak Electronic Coupling.

Application to the Low-Lying States of Mo2Cl84-. *J. Chem. Phys.* **1979**, *70* (11).

(41)   Bruschi, M.; Greco, C.; Fantucci, P.; Gioia, L. De. Structural and Electronic Properties of the [FeFe] Hydrogenase H-Cluster in Different Redox and Protonation States. A DFT Investigation. *Inorg. Chem.* **2008**, *47* (13), 6056–6071 DOI: 10.1021/ic8006298.

(42)   Bruschi, M.; Greco, C.; Kaukonen, M.; Fantucci, P.; Ryde, U.; De Gioia, L. Influence of the [2Fe]H Subcluster Environment on the Properties of Key Intermediates in the Catalytic Cycle of [FeFe] Hydrogenases: Hints for the Rational Design of Synthetic Catalysts. *Angew. Chemie Int. Ed.* **2009**, *48* (19), 3503–3506 DOI: 10.1002/anie.200900494.

(43)   Sensi, M.; Baffert, C.; Greco, C.; Caserta, G.; Gauquelin, C.; Saujet, L.; Fontecave, M.; Roy, S.; Artero, V.; Soucaille, P.; Meynial-Salles, I.; Bottin, H.; de Gioia, L.; Fourmond, V.; Léger, C.; Bertini, L. Reactivity of the Excited States of the H-Cluster of FeFe Hydrogenases. *J. Am. Chem. Soc.* **2016**, *138* (41), 13612–13618 DOI: 10.1021/jacs.6b06603.

(44)   Yamaguchi, K.; Jensen, F.; Dorigo, A.; Houk, K. N. A Spin Correction Procedure for Unrestricted Hartree-Fock and Møller-Plesset Wavefunctions for Singlet Diradicals and Polyradicals. *Chem. Phys. Lett.* **1988**, *149* (5), 537–542 DOI: http://dx.doi.org/10.1016/0009-2614(88)80378-6.

(45)   Lee, C.; Yang, W.; Parr, R. G. Development of the Colle-Salvetti Correlation-Energy Formula into a Functional of the Electron Density. *Phys. Rev. B* **1988**, *37* (2), 785–789 DOI: 10.1103/PhysRevB.37.785.

(46)   Holm, R. H.; Kennepohl, P.; Solomon, E. I. Structural and Functional Aspects of Metal Sites in Biology. *Chem. Rev.* **1996**, *96* (7), 2239–2314 DOI: 10.1021/cr9500390.

(47)   Shook, R. L.; Borovik, A. S. Role of the Secondary Coordination Sphere in Metal-Mediated Dioxygen Activation. *Inorg. Chem.* **2010**, *49* (8), 3646–3660 DOI: 10.1021/ic901550k.

(48)   Span, E. A.; Suess, D. L. M.; Deller, M. C.; Britt, R. D.; Marletta, M. A. The Role of the

Secondary Coordination Sphere in a Fungal Polysaccharide Monooxygenase. *ACS Chem. Biol.* **2017** DOI: 10.1021/acschembio.7b00016.

(49)   Gudmundsson, M.; Kim, S.; Wu, M.; Ishida, T.; Momeni, M. H.; Vaaje-Kolstad, G.; Lundberg, D.; Royant, A.; Stahlberg, J.; Eijsink, V. G. H.; Beckham, G. T.; Sandgren, M. Structural and Electronic Snapshots during the Transition from a Cu(II) to Cu(I) Metal Center of a Lytic Polysaccharide Onooxygenase by X-Ray Photoreduction. *J. Biol. Chem.* **2014**, *289* (27), 18782–18792 DOI: 10.1074/jbc.M114.563494.

(50)   Beeson, W. T.; Phillips, C. M.; Cate, J. H.; Marletta, M. A. Oxidative Cleavage of Cellulose by Fungal Copper-Dependent Polysaccharide Monooxygenases. *J Am Chem Soc* **2012**, *134* DOI: 10.1021/ja210657t.

(51)   Agger, J. W.; Isaksen, T.; Várnai, A.; Vidal-Melgosa, S.; Willats, W. G. T.; Ludwig, R.; Horn, S. J.; Eijsink, V. G. H.; Westereng, B. Discovery of LPMO Activity on Hemicelluloses Shows the Importance of Oxidative Processes in Plant Cell Wall Degradation. *Proc. Natl. Acad. Sci. U. S. A.* **2014**, *111* (17), 6287–6292 DOI: 10.1073/pnas.1323629111.

(52)   Cannella, D.; Möllers, K. B.; Frigaard, N.-U.; Jensen, P. E.; Bjerrum, M. J.; Johansen, K. S.; Felby, C. Light-Driven Oxidation of Polysaccharides by Photosynthetic Pigments and a Metalloenzyme. *Nat. Commun.* **2016**, *7*, 11134.

(53)   Dell, W. B. O.; Agarwal, P. K.; Meilleur, F. Oxygen Activation at the Active Site of a Fungal Lytic Polysaccharide Monooxygenase. *Angew. Chemie (International ed.)* **2016**, *56*, 767–770 DOI: 10.1002/anie.201610502.

(54)   Baik, M. H.; Newcomb, M.; Friesner, R. A.; Lippard, S. J. Mechanistic Studies on the Hydroxylation of Methane by Methane Monooxygenase. *Chem. Rev.* **2003**, *103* (6), 2385–2419 DOI: 10.1021/cr950244f.

(55)   Dhar, D.; Tolman, W. B. Hydrogen Atom Abstraction from Hydrocarbons by a Copper(III)-

Hydroxide Complex. *J. Am. Chem. Soc.* **2015**, *137* (3), 1322–1329 DOI: 10.1021/ja512014z.

(56) Dhar, D.; Yee, G. M.; Spaeth, A. D.; Boyce, D. W.; Zhang, H.; Dereli, B.; Cramer, C. J.; Tolman, W. B. Perturbing the Copper(III)–Hydroxide Unit through Ligand Structural Variation. *J. Am. Chem. Soc.* **2016**, *138* (1), 356–368 DOI: 10.1021/jacs.5b10985.

(57) Scott, B. R.; Huang, H. Z.; Frickman, J.; Halvorsen, R.; Johansen, K. S. Catalase Improves Saccharification of Lignocellulose by Reducing Lytic Polysaccharide Monooxygenase-Associated Enzyme Inactivation. *Biotechnol. Lett.* **2016**, *38* (3), 425–434 DOI: 10.1007/s10529-015-1989-8.

(58) Kracher, D.; Scheiblbrandner, S.; Felice, A. K. G.; Breslmayr, E.; Preims, M.; Ludwicka, K.; Haltrich, D.; Eijsink, V. G. H.; Ludwig, R. Extracellular Electron Transfer Systems Fuel Cellulose Oxidative Degradation. *Science (80-.).* **2016**, *352* (6289), 1098–1101.

(59) Aachmann, F. L.; Sørlie, M.; Skjåk-Bræk, G.; Eijsink, V. G. H.; Vaaje-Kolstad, G. NMR Structure of a Lytic Polysaccharide Monooxygenase Provides Insight into Copper Binding, Protein Dynamics, and Substrate Interactions. *Proc. Natl. Acad. Sci. U. S. A.* **2012**, *109* (46), 18779–18784 DOI: 10.1073/pnas.1208822109.

(60) Lewis, E. A.; Tolman, W. B. Reactivity of Dioxygen-Copper Systems. *Chem. Rev.* **2004**, *104* (2), 1047–1076 DOI: 10.1021/cr020633r.

For Table of Contents Only
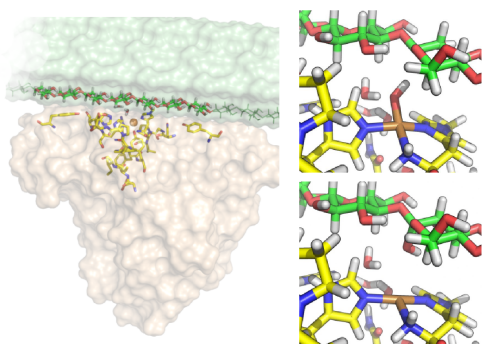
The catalytic mechanism of fungal AA9 LPMOs was elucidated using DFT calculations: hydrogen atom abstraction is performed by a copper oxyl intermediate, and the substrate is hydroxylated via water assisted hydroxyl rebound.